Interlink between Abnormal Water Imbibition in Hydrophilic and Rapid Flow in Hydrophobic Nanochannels

Runfeng Zhou,[1] Mehdi Neek-Amal,[2,3] Francois M. Peeters,[3,4] Bofeng Bai,[1] and Chengzhen Sun[1,*]
[1]State Key Laboratory of Multiphase Flow in Power Engineering, Xi'an Jiaotong University, Xi'an, Shaanxi 710049, China
[2]Department of Physics, Shahid Rajaee Teacher Training University, 16875-163 Lavizan, Tehran, Iran
[3]Departement Fysica, Universiteit Antwerpen, Groenenborgerlaan 171, B-2020 Antwerpen, Belgium
[4]Departamento de Física, Universidade Federal do Ceará, Fortaleza-CE 60455-760, Brazil

(Received 22 December 2023; revised 29 February 2024; accepted 21 March 2024; published 30 April 2024)

Nanoscale extension and refinement of the Lucas-Washburn model is presented with a detailed analysis of recent experimental data and extensive molecular dynamics simulations to investigate rapid water flow and water imbibition within nanocapillaries. Through a comparative analysis of capillary rise in hydrophilic nanochannels, an unexpected reversal of the anticipated trend, with an abnormal peak, of imbibition length below the size of 3 nm was discovered in hydrophilic nanochannels, surprisingly sharing the same physical origin as the well-known peak observed in flow rate within hydrophobic nanochannels. The extended imbibition model is applicable across diverse spatiotemporal scales and validated against simulation results and existing experimental data for both hydrophilic and hydrophobic nanochannels.

DOI: 10.1103/PhysRevLett.132.184001

Introduction.—The phenomenon of spontaneous water flow involves the migration of water into nanochannels (NCs) driven by capillary forces. In recent years, this phenomenon has garnered significant attention, driven by both fundamental physics and potential applications [1,2]. Recent reports have explored water transport through hydrophilic (HPI) and hydrophobic (HPO) NCs, spanning confinement heights from a single atomic layer (≈0.34 nm) to several dozen atomic planes (∼10 nm) [3–17]. The first set of studies focused on measuring fluid weight loss due to evaporation, primarily water [2–5], while the second set of experiments concentrated on the time-dependent position of the meniscus [6–12].

However, as the characteristic length of the flow domain decreases to the nanoscale and below, the predictive power of conventional theories governing water flow, such as the Hagen-Poiseuille (HP) theory [18], and imbibition flow represented by the Lucas-Washburn (LW) equation [6,7,19]:

$$x_{\mathrm{LW}} = \sqrt{\frac{h\gamma\cos\theta_e}{3\mu}t} = \sqrt{2\mathcal{D}_{\mathrm{LW}}t}, \tag{1}$$

where x_{LW} is the imbibition length, t is the imbibition time, h is the height of the NCs, γ is the (air-liquid) surface tension, θ_e is the equilibrium contact angle, μ is the (dynamic) viscosity, and $\mathcal{D}_{\mathrm{LW}} \equiv (h\gamma\cos\theta_e/6\mu)$ is a defined characteristic transport coefficient which has the units of diffusion coefficient, hereafter referred to as the imbibition coefficient, reaches its limitations. An accurate description of water flow and spontaneous imbibition at the nanoscale remains a formidable challenge [18,20–22].

For example, a notable departure from the predictions of the aforementioned classical theories regarding both imbibition length and water weight loss rate becomes increasingly pronounced as the confinement size decreases. This trend is evident in various sets of experimental data, as one typical set demonstrated for HPI channels in Fig. 1. The shaded area signifies the range of NC heights where experimental data are notably scarce, especially below 10 nm. Furthermore, a sequence of studies concentrating on water transport through HPO graphene NCs and carbon

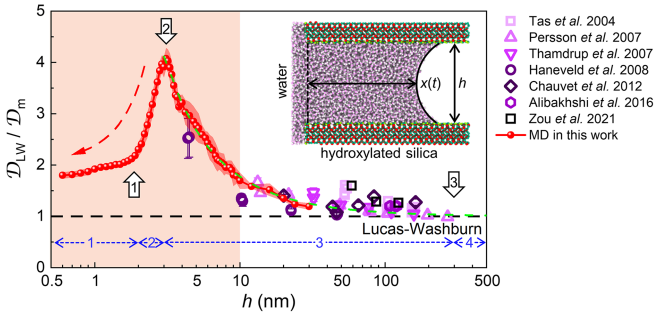

FIG. 1. Deviations in the ratio between the traditional LW equation (black dashed horizontal line) at various channel heights for both experimental and MD data of HPI NCs. The green dashed line represents the descending behavior and deviation from the classical limit (i.e., black dashed line), becoming particularly evident starting from 300 nm and extending down to around and below 10 nm. The red dashed arrow serves as a guide to the eye, emphasizing the deviation from the classical prediction below 3 nm. The arrows indicate distinct regimes. Inset: side view of the water imbibition meniscus in the MD simulation setup, represented by the black curve.

nanotubes has underscored the substantial influence of disjoining pressure in confined, narrow channels, highlighting the constraints of classical HP equations [3,18,22]. Particularly, in situations where channels have a restricted capacity for water layers, this phenomenon is traditionally referred to as "rapid water flow through nanocapillaries" [3,4,23,24]. The observed deviation can be attributed to a myriad of factors, each contributing to intricate and significant nanoconfinement effects on fluids [6–8,14,17].

In this Letter, we present a refined version of the LW equation aimed at elucidating a diverse range of experimental observations in both frictional loss and frictionless NCs, including recent findings on water flow and imbibition [4]. This adaptation, validated through extensive molecular dynamics (MD) simulations on HPI silica NCs (0.6–30 nm in height) and informed by previous MD work on HPO graphene NCs [3,25], incorporates crucial factors such as enhanced viscosity and disjoining pressure. Our analysis of HPI NCs has significantly influenced our approach to the study of HPO NCs, prompting a reexamination of the long-standing puzzle posed by rapid water flow through HPO NCs.

We systematically compare our modified Lucas-Washburn (MLW) equation with diverse experimental data obtained from both HPI and HPO NCs. The primary objective is to establish a direct correlation between these observations, thereby extending the applicability of the LW equation to various NC types. The HP equation serves to model viscous flow in channels, incorporating parameters such as viscosity, pressure gradient, and channel dimensions. In contrast, the LW equation characterizes capillary imbibition, relying on factors like viscosity, equilibrium contact angle, and channel geometry. It is noteworthy that both models emerge as a consequences of the Navier-Stokes equation.

The model and method.—Our nonequilibrium MD simulations are carried out using LAMMPS molecular dynamics simulator [26,27], within a simulation box measuring $L_x \times L_y = 75\ \text{nm} \times 2.5\ \text{nm}$. The dimensions of the box are adjusted to accommodate the varying NC heights (h), ranging from 0.6 nm to 30 nm. The NCs are constructed from hydroxylated silica layers with dimensions $d_x \times d_y \times d_z = 34\ \text{nm} \times 2.5\ \text{nm} \times 1.6\ \text{nm}$, separated by h, as illustrated in the inset of Fig. 1. Silica layers are obtained by cleaving α-quartz crystal planes (001) [28,29], ensuring HPI conditions [30–32]. The simulation uses the consistent valence force field [33] for silica NCs and the SPC/Fw model for water molecules [34,35]. Interactions are represented using the 12-6 Lennard-Jones potential with Coulombic interactions and a cutoff distance of 1 nm. Periodic boundaries, a time step of 1 fs, and temperature control at 300 K using the Nosé-Hoover thermostat connected to water and hydroxyl groups are applied. Initial equilibration includes a nonvisual force wall between the NC entrance and bulk water for 5 ns, followed by a 10 ns trajectory sampling simulation. For more details, see Supplemental Material, Sec. SM-I [36].

The determination of imbibition length in NCs requires discretization of the water domain, computation of water density, interface identification, and meniscus shape determination [37]. The typical imbibition length, denoted as $x(t)$ and defined as the distance between the NC entrance and the bottom of the meniscus curve, is illustrated in the inset of Fig. 1. For more details, see Supplemental Material, Sec. SM-II [36].

Deviation from the LW equation in frictional loss NCs.—In Fig. 2(a) (and Supplemental Material, Fig. S3), we depict the MD data for the temporal evolution of the square of the imbibition length, $x^2(t)$, within hydroxylated silica NCs of varying heights. Notably, in wider NCs, $x^2(t)$ exhibits a subtle deviation from the linear relationship during the initial stages. This initial deviation can be primarily attributed to three key factors: the inertia effect [38], the dynamic contact angle effect [39–42], and the entrance effect [43,44]. While the inertia effect tends to rapidly diminish within tens of picoseconds [45], the more prolonged deviation predominantly results from the dynamic contact angle and the entrance effect. The presence of a nonlinear relationship during the initial stages suggests that factors beyond viscosity may significantly influence nanoscale imbibition dynamics. For more discussions on dynamic contact angle, see Supplemental Material, Sec. SM-V [36].

Significantly, in narrower NCs, the measured imbibition coefficient ($\mathcal{D}_\text{m}$) as well as the imbibition length (x) closely conforms to LW predictions, as is evident from the curved red dashed arrow in Fig. 1. This intriguing outcome contradicts the expected trend based on previous experimental data in Fig. 1 [6–12], where deviations in $(\mathcal{D}_\text{LW}/\mathcal{D}_\text{m})$ were anticipated to increase as channel height decreases, as indicated by the green dashed line in Fig. 1. Comparing our simulation results with existing experimental data, we conclude that the deviation in imbibition coefficient and the corresponding imbibition length exhibits a nonmonotonic variation with h. Consistent results are obtained using different MD strategies, as described in Supplemental Material, Sec. SM-VIII [36,44,46–49].

The ratio between $\mathcal{D}_\text{LW}$ from original LW equation and $\mathcal{D}_\text{m}$ from MD data presented in Fig. 1 highlights the complex nature of water transport in silica NCs, particularly when h is below 10 nm. The existing experimental data within this h range are limited, with only sparse information around $h = 5$ nm, posing challenges for drawing definitive conclusions. Technical constraints in measuring imbibition length for channels below 10 nm further compound the issue, underscoring the necessity for additional experimental and MD data to facilitate an accurate comparison.

To analyze the height scales comprehensively, we categorize them into four distinct ranges: (i) $h < 2$ nm,

(ii) $2 < h < 3$ nm, (iii) $3 < h < 300$ nm, and (iv) $h > 300$ nm. In the last segment, nanoscale effects can be disregarded and the LW equation works well. In the other ranges, the confinement effect becomes prominent and leads to an increase in effective viscosity, and significant deviations are observed, with a profound peak around 3 nm. Below this, the short-range disjoining pressure becomes prominent and enhances imbibition while compensating for nanoscale flow, and a rapid decrease in deviation is evident until 2 nm, where the compensation effect of disjoining pressure on viscosity weakens and a slower decrease is observed.

Modified LW equation.—In alignment with our approach for HPO NCs [18], we introduce modifications to the LW equation. These modifications incorporate an effective viscosity term [50], denoted as μ_h, which varies with h. This approach diverges from conventional bulk viscosity [51], denoted as μ_b, and is defined as follows: $\mu_h = \mu_b(1 + \mu_0 e^{-h/\lambda})$. Here, μ_0 and λ are characteristic parameters [4,18], and $\mu_b = 0.89$ mPa s represents the viscosity of bulk water at room temperature (more details in Supplemental Material, Sec. SM-III [36]).

Additionally, while taking into account Laplace's pressure and the viscous pressure drop within the NCs, we introduce the disjoining pressure (P_d) [3,18,23,52,53] which is the pressure difference between the water inside the NC and outside the channel. Therefore, the total driving pressure for liquid flow can be approximated as $P = P_c + P_d$, where $P_c = (2\gamma \cos\theta_e/h)$ represents the capillary pressure in the classical regime. It is worth noting that P_d characterizes the water-surface interaction, which can dominate at the nanoscale but decreases rapidly with increasing h. We can express it as $P_d \approx \pi_d e^{-h/\lambda'}$ [52–55] (more details in Supplemental Material, Sec. SM-IV [36]) as illustrated in Figs. 2(b) and 2(c) for HPI NCs, while for HPO NCs, it was studied in Refs. [3,18] (see Supplemental Material, Fig. S7 with more details in Sec. SM-VII [36]).

In addition to the aforementioned corrections for viscosity and disjoining pressure, we further extend the LW equation by multiplying pressure with $1 + (6\delta/h)$, which takes into account the well-known slip term [56–60]. Here, δ represents the slip length, which can be negligible (small) for HPI silica (hexagonal boron nitride, h-BN) NCs. Consequently, the LW equation can be approximated for long times ($t \gg 1$ μs) as follows:

$$x_{\mathrm{MLW}} \approx \sqrt{\frac{h^2}{6}\frac{P}{\mu_h}\left(1 + \frac{6\delta}{h}\right)t}. \tag{2}$$

Under these conditions, Eq. (2) converges to the original LW equation for microchannels, aligning with experimental observations. However, for NCs, adjustments to $\mathcal{D}$ (that is, P and μ) are necessary. Further insights, a complete form of the MLW equation and a detailed analysis of the long-time approximation of Eq. (2) can be found in Supplemental Material, Sec. SM-VI [36]. A comprehensive list of various modifications to LW equation can be found in the literature [21,44,61]. By incorporating parameters derived from our or others' MD simulations (Table I), we achieve close agreement between the predicted imbibition length and MD and experimental results in both narrow and wide channels at $t = 100$ s. For instance, in Fig. 2(c) [and Fig. S7(b)], we illustrate the impact of varying π_d in Eq. (2) within the range of 0–20 kbar (with the provided parameters in Table I) to explain the nonmonotonic deviation in imbibition length. The appearance of disjoining pressure compensates the large deviation resulting from the enhanced viscosity (more details in Secs. SM-III and SM-IV [36]).

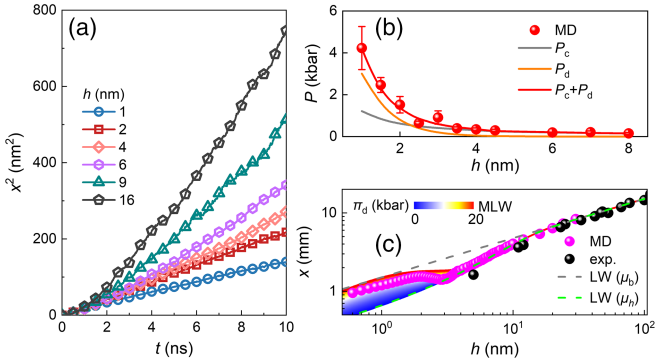

FIG. 2. (a) Temporal evolution of the square of the imbibition length x^2. (b) Different type of driving pressures as a function of height. (c) Influence of the disjoining pressure parameter (π_d) on the imbibition length of water in HPI silica nanochannels.

In this Letter, the parameters for refining the LW equation were determined based on MD simulation data from silica, as well as previous simulations on graphene and h-BN [3,18,25]. The results indicate a narrow parameter range around the values obtained from MD simulations, as shown in Table I. For example, equilibrium contact angles for silica, graphene, and h-BN are approximately 15°, 89.95°, and 89°, respectively, and the π_d values are a few kilobars, aligning with established values. It is crucial to note that these parameters fall within the expected range. Given the broad spectrum of h and timescales considered in our study, demanding highly precise parameter values exceeds the bounds of physical intuition.

TABLE I. The parameters employed in MLW model for different NCs. Parameters for graphene are derived from both our current and previous studies [3,18,25].

Channel	θ_e (°)	μ_0	λ (nm)	π_d (kbar)	λ' (nm)
Graphene	89.5–90	~1000	0.1–0.6 [18]	~3 [3]	~0.5
h-BN	86.5–89.5	~4.8	~4	~5	~0.36
Silica	0–60	4.8	4.1	11.37	0.72

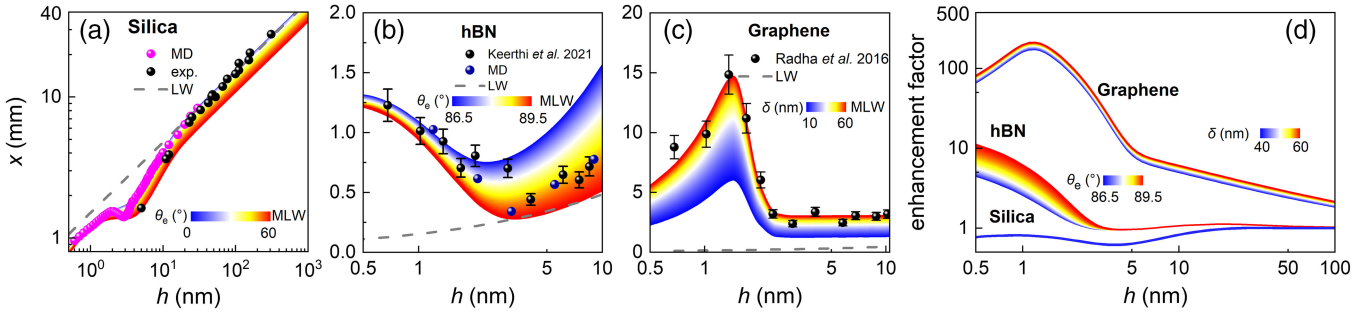

FIG. 3. The imbibition lengths for silica (a) and h-BN (b), determined by x_{MLW}, vary with equilibrium contact angles within the range of 0–60 degrees for silica and 86.5–89.5 degrees for h-BN (indicated by color bars), respectively. Panel (c) shows the imbibition length variations for graphene with different slip lengths within the range of 10–60 nm. Experimental data obtained from various literature sources, as explained in the main text, is represented by dots. The dashed gray lines represent the results of the original LW equation. (d) The variation of enhancement factor ($\epsilon = (x_{\mathrm{MLW}}/x_{\mathrm{LW}})$) with the channel height.

Modified LW model for experimental data of water flow through HPI/HPO NCs.—We consolidate the reliability of our model [Eq. (2)] by conducting a comprehensive examination of experimental data from the literature. This analysis includes studies on water imbibition into silica NCs [6–10,14], as well as h-BN NCs [4]. Figure 3(a) provides a comprehensive comparative analysis of our MD results (magenta dots) with theoretical predictions from the original (gray dashed line) and MLW equations using parameters from the third row of Table I and $\delta = 0$ nm for silica (color spectrum), showing a close agreement among experimental data, MD and MLW for heights ranging from 0.6 nm to 1 μm and equilibrium contact angles represented by color bars within the range of 0–60°. While elements of our modification can be found in existing literature, our work's significance lies in uniting studies on HPO and HPI NCs.

Next, we delve into the experimental aspect of our study, where we integrate experimental measurements and link them with both MLW and MD methods. The aim is to transform weight loss rate data, widely used in recent experiments [3,4], into imbibition length data. This breakthrough not only fills a crucial gap in nanofluidic research but also lays the foundation for a theoretical framework that could revolutionize nanofluidic measurements. The weight loss rate data, represented as $Q = \rho whV$, where ρ, w denoting the density and channel width and V the streamline velocity in a channel with length L, can be related to imbibition length data through imbibition velocity $(\mathrm{d}x/\mathrm{d}t)|_{x=L} = (\mathcal{D}/L)$ using the defined imbibition coefficient $\mathcal{D} = (x^2/2t)$, where

$$V|_{x=L} = \frac{Q}{\rho wh} = \frac{\mathcal{D}}{L}. \tag{3}$$

By determining the value of $\mathcal{D}$, one is able to calculate experimental values for $x = \sqrt{2(QL/\rho wh)t}$.

In Figs. 3(b) and 3(c), we made the conversion of weight loss data obtained from h-BN and graphene NCs. We used $\delta = 1$ nm to represent h-BN and $\delta = 60$ nm for graphene, which are values extracted from Ref. [4]. The colored spectrum elegantly depicts the results of x_{MLW}, showing exceptional agreement with experimental observations (black dots). For comparison, additional MD simulations give imbibition results in the h-BN NCs [navy dots in Fig. 3(b) with a shift], showing agreement with experiment and proposed MLW model. These results were obtained using the parameters provided in Table I, primarily derived from MD simulations. Notably, for both h-BN and graphene, equilibrium contact angles close to 90° yield excellent agreement.

The differences observed between graphene and h-BN, as indicated by the varying δ values, stem from the distinct water adsorption behaviors in HPI channels. Specifically, from Fig. 3(b), it is evident that the equilibrium contact angles should be close to 90° even for large h in h-BN NCs. Additionally, Fig. 3(c) illustrates that $\delta = 60$ nm in graphene NCs results in excellent agreement with experiments for $h < 2$–3 nm. However, beyond this range of heights, no significant effects are observed.

Eventually, we calculate the water imbibition enhancement factor, denoted as $\epsilon = (x_{\mathrm{MLW}}/x_{\mathrm{LW}})$. The enhancement of flow has been extensively documented in studies involving water transport through carbon nanotubes [62–65]. In Fig. 3(d), we present the variation of ϵ with h. Remarkably, a substantial 2-orders-of-magnitude reduction in ϵ is observed from graphene (with $\theta_e = 89.95°$) to h-BN (with $\theta_e = 89°$) at $h \approx 1.4$ nm. Even with this reduction, h-BN demonstrates significant faster flow compared to silica. This notable decrease in ϵ between graphene and h-BN is consistent with experimental findings in weight loss measurements [4], underscoring a profound interlink between weight loss measurements and imbibition length identification. We term this intricate relationship as the "interlink" between these phenomena, revealing a previously unexplored facet of nanofluidic dynamics. Moreover, in silica, when the height $h < 50$ nm, we observe a decrease in ϵ (where $\epsilon < 1$) due to enhanced viscosity. Notably, as the height h decreases to

2–3 nm, the enhancement factor rises owing to the emergence of disjoining pressure.

Moreover, we can extend this approach to nanotubes with radius denoted as r by adapting the LW equation as follows: $x_{\mathrm{MLW}} \approx \sqrt{(Pr^2/4\mu_r)[1+(4\delta/r)]t}$, where P and μ_r represent radius-dependent pressure and viscosity, respectively.

In summary, we presented a generalization of the LW equation that included enhanced viscosity, disjoining pressure, and slip conditions in both HPO and HPI NCs. Our model is valid over spatial scales from nanometers to hundreds of nanometers and temporal scales spanning from nanoseconds to hours. Thus, our model provides a unified framework for comprehending and predicting the spontaneous imbibition of fluids within channels. This modified equation was rigorously validated against MD results and existing experimental data, accurately forecast imbibition dynamics within NCs. Notably, our model effectively addresses wall slip effects, particularly in graphene NCs.

We gratefully acknowledge the financial support provided by the National Natural Science Foundation of China (Projects No. 52488201 and No. 52222606). Part of this project was supported by the Flemish Science Foundations (FWO-Vl) and the Iranian National Science Foundation (No. 4025061 and No. 4021261).

*sun-cz@xjtu.edu.cn

[1] C. Sun, R. Zhou, Z. Zhao, and B. Bai, J. Phys. Chem. Lett. **11**, 4678 (2020).
[2] Y. You, A. Ismail, G.-H. Nam, S. Goutham, A. Keerthi, and B. Radha, Annu. Rev. Mater. Res. **52**, 189 (2022).
[3] B. Radha, A. Esfandiar, F. Wang, A. Rooney, K. Gopinadhan, A. Keerthi, A. Mishchenko, A. Janardanan, P. Blake, L. Fumagalli *et al.*, Nature (London) **538**, 222 (2016).
[4] A. Keerthi, S. Goutham, Y. You, P. Iamprasertkun, R. A. Dryfe, A. K. Geim, and B. Radha, Nat. Commun. **12**, 3092 (2021).
[5] S. Goutham, A. Keerthi, A. Ismail, A. Bhardwaj, H. Jalali, Y. You, Y. Li, N. Hassani, H. Peng, M. V. S. Martins *et al.*, Nat. Nanotechnol. **18**, 596 (2023).
[6] N. R. Tas, J. Haneveld, H. V. Jansen, M. Elwenspoek, and A. van den Berg, Appl. Phys. Lett. **85**, 3274 (2004).
[7] F. Persson, L. H. Thamdrup, M. B. L. Mikkelsen, S. Jaarlgard, P. Skafte-Pedersen, H. Bruus, and A. Kristensen, Nanotechnology **18**, 245301 (2007).
[8] L. H. Thamdrup, F. Persson, H. Bruus, A. Kristensen, and H. Flyvbjerg, Appl. Phys. Lett. **91**, 163505 (2007).
[9] J. Haneveld, N. R. Tas, N. Brunets, H. V. Jansen, and M. Elwenspoek, J. Appl. Phys. **104**, 014309 (2008).
[10] F. Chauvet, S. Geoffroy, A. Hamoumi, M. Prat, and P. Joseph, Soft Matter **8**, 10738 (2012).
[11] M. A. Alibakhshi, Q. Xie, Y. Li, and C. Duan, Sci. Rep. **6**, 24936 (2016).
[12] A. Zou, S. Poudel, M. Gupta, and S. C. Maroo, Nano Lett. **21**, 7769 (2021).
[13] K. M. van Delft, J. C. Eijkel, D. Mijatovic, T. S. Druzhinina, H. Rathgen, N. R. Tas, A. van den Berg, and F. Mugele, Nano Lett. **7**, 345 (2007).
[14] N. A. Mortensen and A. Kristensen, Appl. Phys. Lett. **92**, 063110 (2008).
[15] S. Gruener, T. Hofmann, D. Wallacher, A. V. Kityk, and P. Huber, Phys. Rev. E **79**, 067301 (2009).
[16] J. W. Van Honschoten, N. Brunets, and N. R. Tas, Chem. Soc. Rev. **39**, 1096 (2010).
[17] Q. Xie, M. A. Alibakhshi, S. Jiao, Z. Xu, M. Hempel, J. Kong, H. G. Park, and C. Duan, Nat. Nanotechnol. **13**, 238 (2018).
[18] M. Neek-Amal, A. Lohrasebi, M. Mousaei, F. Shayeganfar, B. Radha, and F. M. Peeters, Appl. Phys. Lett. **113**, 083101 (2018).
[19] E. W. Washburn, Phys. Rev. **17**, 273 (1921).
[20] W.-J. Plug and J. Bruining, Adv. Water Resour. **30**, 2339 (2007).
[21] J. Cai, T. Jin, J. Kou, S. Zou, J. Xiao, and Q. Meng, Langmuir **37**, 1623 (2021).
[22] S. K. Kannam, B. Todd, J. S. Hansen, and P. J. Daivis, J. Chem. Phys. **138** (2013).
[23] S. Gravelle, C. Ybert, L. Bocquet, and L. Joly, Phys. Rev. E **93**, 033123 (2016).
[24] S. K. Kannam, B. Todd, J. S. Hansen, and P. J. Daivis, J. Chem. Phys. **135**, 144701 (2011).
[25] M. Neek-Amal, F. M. Peeters, I. V. Grigorieva, and A. K. Geim, ACS Nano **10**, 3685 (2016).
[26] S. Plimpton, J. Comput. Phys. **117**, 1 (1995).
[27] A. P. Thompson, H. M. Aktulga, R. Berger, D. S. Bolintineanu, W. M. Brown, P. S. Crozier, P. J. in't Veld, A. Kohlmeyer, S. G. Moore, T. D. Nguyen *et al.*, Comput. Phys. Commun. **271**, 108171 (2022).
[28] Y. Yan, Z. Dong, Y. Zhang, P. Wang, T. Fang, and J. Zhang, Phys. Chem. Chem. Phys. **19**, 30439 (2017).
[29] Y. Zhang and W. Guo, Fuel **293**, 120428 (2021).
[30] A. Skelton, P. Fenter, J. D. Kubicki, D. J. Wesolowski, and P. T. Cummings, J. Phys. Chem. C **115**, 2076 (2011).
[31] Q. Liu, S. Yuan, H. Yan, and X. Zhao, J. Phys. Chem. B **116**, 2867 (2012).
[32] H. Sun, W. Sun, H. Zhao, Y. Sun, D. Zhang, X. Qi, and Y. Li, RSC Adv. **6**, 32770 (2016).
[33] A. Hagler, E. Huler, and S. Lifson, J. Am. Chem. Soc. **96**, 5319 (1974).
[34] Y. Wu, H. L. Tepper, and G. A. Voth, J. Chem. Phys. **124**, 024503 (2006).
[35] A. Markesteijn, R. Hartkamp, S. Luding, and J. Westerweel, J. Chem. Phys. **136** (2012).
[36] See Supplemental Material at http://link.aps.org/supplemental/10.1103/PhysRevLett.132.184001 for simulation details, including the determination of imbibition length, channel height, contact angle, the effect of thermostat procedure and wall constraint, as well as further discussions on viscosity, disjoining pressure, dynamic contact angle, the complete form of the modified model, and imbibition in hydrophobic nanochannels.
[37] G. J. Wang, A. Damone, F. Benfenati, P. Poesio, G. P. Beretta, and N. G. Hadjiconstantinou, Phys. Rev. Fluids **4**, 124203 (2019).

[38] C. Bosanquet, London, Edinburgh, Dublin Philos. Mag. J. Sci. **45**, 525 (1923).
[39] G. Martic, F. Gentner, D. Seveno, D. Coulon, J. De Coninck, and T. Blake, Langmuir **18**, 7971 (2002).
[40] T. D. Blake and J. M. Haynes, J. Colloid Interface Sci. **30**, 421 (1969).
[41] S. Glasstone, K. J. Laidler, and H. Eyring, *The Theory of Rate Processes* (McGraw-Hill, New York, 1941).
[42] M. J. de Ruijter, T. D. Blake, and J. De Coninck, Langmuir **15**, 7836 (1999).
[43] R. Zhou, Z. Qiu, C. Sun, and B. Bai, Phys. Fluids **35**, 042005 (2023).
[44] M. Heiranian and N. R. Aluru, Phys. Rev. E **105**, 055105 (2022).
[45] E. Oyarzua, J. H. Walther, A. Mejía, and H. A. Zambrano, Phys. Chem. Chem. Phys. **17**, 14731 (2015).
[46] A. Sam, S. K. Kannam, R. Hartkamp, and S. P. Sathian, J. Chem. Phys. **146**, 234701 (2017).
[47] A. Gubbiotti, M. Baldelli, G. Di Muccio, P. Malgaretti, S. Marbach, and M. Chinappi, Adv. Phys. **7**, 2036638 (2022).
[48] S. Bhattacharya, J. Muzard, L. Payet, J. Mathé, U. Bockelmann, A. Aksimentiev, and V. Viasnoff, J. Phys. Chem. C **115**, 4255 (2011).
[49] S. Supple and N. Quirke, Phys. Rev. Lett. **90**, 214501 (2003).
[50] R. C. Major, J. E. Houston, M. J. McGrath, J. I. Siepmann, and X.-Y. Zhu, Phys. Rev. Lett. **96**, 177803 (2006).
[51] R. Zhou, C. Sun, and B. Bai, J. Chem. Phys. **154**, 074709 (2021).
[52] J. N. Israelachvili, *Intermolecular and Surface Forces*, 3rd ed. (Academic Press, San Diego, 2011).
[53] V. M. Starov and M. G. Velarde, *Wetting and Spreading Dynamics*, 2nd ed., (CRC Press, Boca Raton, 2019), 10.1201/9780429506246.
[54] P. A. Kralchevsky and N. D. Denkov, Chem. Phys. Lett. **240**, 385 (1995).
[55] M. Svoboda, F. Moučka, and M. Lísal, J. Mol. Liq. **271**, 490 (2018).
[56] L. Fu, S. Merabia, and L. Joly, Phys. Rev. Lett. **119**, 214501 (2017).
[57] Y. Xie, L. Fu, T. Niehaus, and L. Joly, Phys. Rev. Lett. **125**, 014501 (2020).
[58] D. Schebarchov and S. C. Hendy, Phys. Rev. E **78**, 046309 (2008).
[59] D. I. Dimitrov, A. Milchev, and K. Binder, Phys. Rev. Lett. **99**, 054501 (2007).
[60] M. E. Suk and N. R. Aluru, Nanoscale Microscale Thermophys. Eng. **21**, 247 (2017).
[61] S. B. Lunowa, A. Mascini, C. Bringedal, T. Bultreys, V. Cnudde, and I. S. Pop, Langmuir **38**, 1680 (2022).
[62] A. Sam, R. Hartkamp, S. Kumar Kannam, J. S. Babu, S. P. Sathian, P. J. Daivis, and B. Todd, Mol. Simul. **47**, 905 (2021).
[63] M. Heiranian and N. R. Aluru, ACS Nano **14**, 272 (2019).
[64] D.-C. Yang, R. J. Castellano, R. P. Silvy, S. K. Lageshetty, R. F. Praino, F. Fornasiero, and J. W. Shan, Nano Lett. **23**, 4956 (2023).
[65] X. Qin, Q. Yuan, Y. Zhao, S. Xie, and Z. Liu, Nano Lett. **11**, 2173 (2011).